Hindawi
Mathematical Problems in Engineering
Volume 2019, Article ID 3926906, 9 pages
https://doi.org/10.1155/2019/3926906

Research Article

Dynamic Modeling and Characteristic Analysis of Cantilever Piezoelectric Bimorph

Heng Chen, Jun-shan Wang, Chao Chen, Shi-xiang Liu, and Hai-peng Chen

State Key Laboratory of Mechanics and Control of Mechanical Structures, Nanjing University of Aeronautics & Astronautics, Nanjing 210016, China

Correspondence should be addressed to Chao Chen; chaochen@nuaa.edu.cn

Received 26 November 2018; Accepted 5 February 2019; Published 3 March 2019

Academic Editor: Gareth A. Vio

The analytical model of an axially precompressed cantilever bimorph is established using the Hamilton's principle in this study, and the static characteristics are obtained. The dynamic equations of the cantilever bimorph in generalized coordinates are established using a numerical method, and the dynamic characteristics are analyzed. Finally, simulations are performed and experiments are conducted to verify the validity of the theory. The results show that increase of axial force has significant amplification effects on the steady-state response amplitude of the displacement, and it reduces the resonance frequency. The response time is still in the millisecond range under a large axial force, which indicates that the bimorph has excellent dynamic characteristics as an actuator.

1. Introduction

With the development of microelectromechanical systems and flight control technology, the miniaturization and intellectualization of unmanned aerial vehicles (UAVs) have attracted increasing attention from researchers [1]. As an important part of the aircraft, the actuator determines the performance of the flight control system [2]. The traditional electromagnetic actuator has many problems, such as a narrow control band, low precision, low energy density, and it has gradually been unable to satisfy the requirements of design and application [3, 4]. Therefore, a new driving mode of control surface is required to solve the problem.

With the rapid development of intelligent materials, researchers are increasingly attempting to apply them to the design and manufacture of aircraft [5, 6]. The energy density and control bandwidth are two important criteria for the actuator of micro air vehicles. Compared with shape memory alloys and magnetostrictive materials, piezoelectric materials, owing to many advantages such as wide band, high energy density, and high conversion rate of mechanical and electrical energy, have become the ideal material for the design of aircraft actuator [7]. As early as 1998, Wlezien R W of the NASA Langley Research Center proposed that piezoelectric materials would be the best choice for the actuator of variant aircraft, but they must overcome the limitation of their small deformation [8].

Piezoelectric bimorph has advantages such as low weight, low power consumption, simple structure, and absence of electromagnetic interference, which is very suitable for the actuator of micro aircraft and intelligent ammunition [9–11]. Owing to the small excitation strain of piezoelectric materials [12], piezoelectric bimorph has the disadvantage of small displacement output. In order to solve this problem, researchers have conducted extensive studies to investigate the characteristics of the bimorph [13, 14], and have proposed various solutions, including various kinds of mechanical magnification mechanisms, such as lever mechanism, planar four bar mechanism, and triangular displacement amplification mechanism [15, 16]. In 1997, Lesieutre proposed the concept of PBP (postbuckled precompressed) [17, 18], which showed that the displacement output and electromechanical conversion efficiency will increase upon applying axial precompression to a piezoelectric bimorph. In theory, the electromechanical coupling factor can reach 100 percent when the axial force is equal to the buckling load. Based on this theory, researchers at Delft University of Technology successfully applied piezoelectric bimorph to the design and manufacture of various aircraft, such as morphing wing UAVs [19] and XQ138 [20]. Moreover, they also used PBP

actuators to optimize the design of the piezoelectric flight control surface [21]. In order to analyze the static and dynamic characteristics of a piezoelectric bimorph under axial precompression, Giannopoulos et al. of the Civil and Materials Engineering Department at the Royal Military Academy used nonlinear mechanics to establish a theoretical model for bimorphs and verified the validity of the analytical model through experiments and simulations [22, 23].

For actuators driven by axially precompressed piezoelectric bimorphs, the characteristics of the bimorphs determine the performance of the actuators. Therefore, it is necessary to definitively describe the static and dynamic characteristics of axially precompressed bimorphs. However, the dynamic expression of the existing precompressed bimorph is not perfect, and the established kinetic model has been significantly simplified. Most of the researchers took the effect of the piezoelectricity as the bending moment when establishing the statics model [19, 20]. For the establishment of the kinetic model, they simplified the bimorph into a single-degree-of-freedom system to obtain the first-order natural frequency [21], but this method could not get the output characteristics of the system at other excitation frequencies. In this paper, the rigid-flexible coupling dynamics model of the bimorph is established based on the finite element method, which can be used to analyze various dynamic characteristics such as amplitude-frequency characteristics of the system. The validity of the model is verified through simulations and experiments, thus providing a theoretical basis for the application of the piezoelectric bimorph.

2. Establishment of Static and Dynamic Model

2.1. Driving Principle of Piezoelectric Bimorphs as Actuators. Piezoelectric bimorph consists of two piezoelectric layers and one substrate layer. As shown in Figure 1, the polarization direction of the two piezoelectric materials is the same. The same voltage signal is connected to the upper and lower surfaces, and the substrate is grounded. The two piezoelectric layers extend and contract respectively so that the bimorph can deform in two directions. If a mechanical device is added at the end of the structure, the bimorph will become an actuator of the servo system.

2.2. Static Model of Axially Precompressed Cantilever Bimorph. The bimorph is simplified to a three-layer Euler beam model without considering the kinetic energy of infinitesimal rotation [24]. The kinetic energy, potential energy, and the work done by the axial force and the electric field are calculated. The following equations can be obtained by considering variation of the energy functionals.

$$\begin{aligned} \delta T_{bi} &= (\rho \mathrm{A}) \int_0^L \dot{w} \delta \dot{w} dx \\ \rho \mathrm{A} &= 2\rho_p A_p + \rho_s A_s, \end{aligned} \tag{1}$$

where δT_{bi} is the variation of the total kinetic energy and ρA represents the linear density of the bimorph. The subscript s and p indicate the substrate and piezoelectricity, respectively. ρ_s and ρ_p are the corresponding density, A_s and A_p are the corresponding cross-sectional area. L represents the length of the bimorph. $\dot{w}$ is the first derivative of the neutral layer deflection versus time.

$$\begin{aligned} \delta U_{bi} &= EI \int_0^L w'' \delta w'' dx + \frac{M_e}{2} \int_0^L \delta w'' dx \\ M_e &= b E_3 d_{31} E_p h_p \left(h_s + h_p\right) \\ EI &= E_s I_s + 2E_p I_p. \end{aligned} \tag{2}$$

δU_{bi} is the variation of the total potential energy and EI represents the bending stiffness of the bimorph. E_s and E_p represent the elastic moduli of the substrate and the piezoelectric layer, respectively. I_s and I_p are the corresponding inertias, h_s and h_p are the corresponding thicknesses. b represents the width of the bimorph, w'' is the second derivative of the neutral layer deflection versus the x-axis. E_3 represents the electric field strength along the z-axis, d_{31} is the piezoelectric constant in the corresponding direction. The following conclusion can be obtained from (2).

$$\begin{aligned} \delta U_{bi} = EI &\left(w'' \ \delta w' \Big|_0^L - w''' \delta w \Big|_0^L + \int_0^L w^{(4)} \delta w dx \right) \\ &+ \frac{1}{2} M_e \ \delta w' \Big|_0^L. \end{aligned} \tag{3}$$

Assuming that the beam is not extensible and the axial pressure F is applied to the beam, the total work of the system can be obtained. The following formula can be achieved by considering the variation of the total work.

$$\delta W = -\frac{1}{2} M_e \ \delta w' \Big|_0^L + F w' \ \delta w \Big|_0^L - F \int_0^L w'' \delta w dx. \tag{4}$$

From the Hamilton's principle, the stationary point of the functional is obtained by

$$\delta \int_{t_1}^{t_2} \left(T_{bi} - U_{bi} + W\right) dt = 0. \tag{5}$$

According to the partial differential equations obtained above, it can be observed that the kinetic equation of the bimorph is consistent with that of the ordinary homogeneous beam. The converse piezoelectric effect is not reflected in the equation but in the boundary condition

$$\rho A \ddot{w} + EI w^{(4)} + F w'' = 0. \tag{6}$$

Assuming that the axial force is always horizontal, the boundary conditions of the cantilever bimorph can be obtained as follows:

$$\begin{aligned} w'' &= \frac{-M_e}{EI}, \quad x = L \\ EI w''' + F w' &= 0, \quad x = L \\ w' &= 0, \quad x = 0 \\ w &= 0, \quad \mathrm{x} = 0. \end{aligned} \tag{7}$$

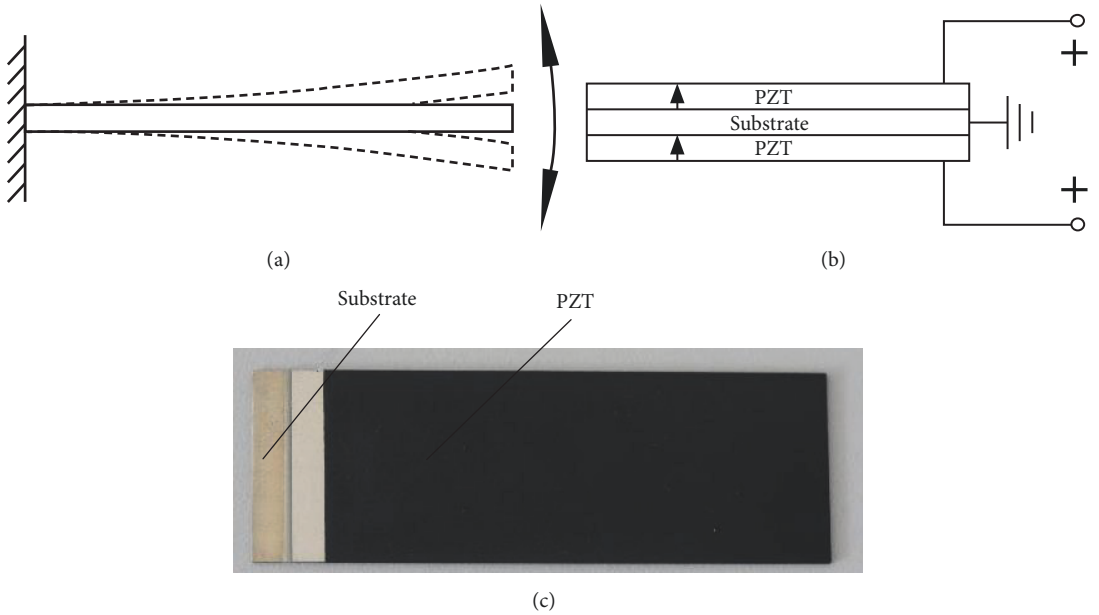

Figure 1: Piezoelectric bimorphs (a) Deformation modes; (b) Connection mode; (c) Structure.

The deflection of the cantilever bimorph is obtained by solving the above formula as follows:

$$w_s = \frac{M_e\left[\cos\left(\lambda x\right) - 1\right]}{F\cos\left(\lambda L\right)}$$
$$\lambda = \sqrt{\frac{F}{EI}}. \tag{8}$$

When the denominator of formula (8) is zero, the first-order buckling critical load of the cantilever bimorph is obtained as

$$F_{cr} = EI\frac{\pi^2}{4L^2}. \tag{9}$$

2.3. Rigid-Flexible Coupling Dynamic Model of Cantilever Bimorph. For the cantilever bimorph, it is difficult to obtain the analytical solution. Therefore, the bimorph can be discretized along the x-axis, and the deflection and rotation angles at both ends of the beam element can be selected as the generalized coordinates. The deflection is assumed to obtain the shape function matrix of the element, and the linear differential equations and element characteristic matrix based on the generalized coordinates are obtained using the Hamilton's principle. Then the integral characteristic matrix of the bimorph is obtained.

The bimorph is dispersed along the x-axis into n units, and the length of each unit is $\Delta x = L/n$. The unit deflection is assumed as [24]

$$w = \left[f\right]^T\left[a\right] = \left[N\right]\left[\delta\right]. \tag{10}$$

Here

$$\left[f\right] = \begin{bmatrix}1 & x & x^2 & x^3\end{bmatrix}^T$$
$$\left[a\right] = \begin{bmatrix}a_1 & a_2 & a_3 & a_4\end{bmatrix}^T, \tag{11}$$

$$\left[\delta\right] = \begin{bmatrix}w_1\\ w_1'\\ w_2\\ w_2'\end{bmatrix} = \begin{bmatrix}1 & 0 & 0 & 0\\ 0 & 1 & 0 & 0\\ 1 & \Delta x & \Delta x^2 & \Delta x^3\\ 0 & 1 & 2\Delta x & 3\Delta x^2\end{bmatrix}\begin{bmatrix}a_1\\ a_2\\ a_3\\ a_4\end{bmatrix} = \left[\Lambda\right]\left[a\right]. \tag{12}$$

From (11) and (12), the shape function matrix of the unit can be calculated as

$$\left[N\right] = \left[f\right]^T\left[\Lambda\right]^{-1}. \tag{13}$$

Therefore, the deflection w can be expressed as a function of the generalized coordinates δ, and the bimorph is simplified as a multi-degree-of-freedom system. Subsequently, the dynamic equation of the unit is built using the Lagrange equation. The kinetic energy, strain energy, potential energy, and work done by the axial force are expressed as a function of the generalized coordinate δ, and the mass matrix, stiffness matrix, and excitation vector are obtained. Here, the kinetic energy of the bimorph element is expressed as

$$T = T_s + 2T_p = \frac{1}{2}\rho A\int_0^{\Delta x}\dot{\delta}^T N^T N\dot{\delta}dx. \tag{14}$$

Here, ρA and EI have the same form as formula (6), except that the length L is replaced by Δx. The expression of the strain energy and electric potential energy of the piezoelectric

material layer can be obtained from the piezoelectric equation. The total strain energy of the unit is as follows:

$$\begin{aligned} U &= U_s + 2U_p \\ &= \frac{1}{2}EI\int_0^{\Delta x}\delta^T N''^T N''\delta dx + \frac{M_e}{2}\begin{bmatrix}0 & -1 & 0 & 1\end{bmatrix}\delta, \end{aligned} \tag{15}$$

where M_e is the equivalent of M_e in (2). Subsequently, the expression of the effect of voltage and axial force on the generalized coordinates is calculated. The electric potential energy is

$$\begin{aligned} W_E = \frac{-M_e}{4}\begin{bmatrix}0 & -1 & 0 & 1\end{bmatrix}\delta - \frac{b\Delta x h_p E_p E_3^2 d_{31}^2}{2} \\ + \frac{b\Delta x h_p E_3^2 \varepsilon_{33}}{2}. \end{aligned} \tag{16}$$

The effect of axial force is

$$W_F = F\int_0^{\Delta x}\frac{w'^2}{2}dx = \frac{F}{2}\int_0^{\Delta x}\delta^T N'^T N'\delta dx. \tag{17}$$

The total work is

$$W = W_F + 2W_E. \tag{18}$$

The linear differential equations are established using the Lagrange equation as follows:

$$\frac{d}{dt}\frac{\partial T}{\partial \dot{\delta}} + \frac{\partial U}{\partial \delta} = \frac{\partial W}{\partial \delta}. \tag{19}$$

The dynamic equation of the element is given by

$$[M]\left\{\ddot{\delta}\right\} + [K]\{\delta\} = M_e\begin{bmatrix}0 & 1 & 0 & -1\end{bmatrix}^T. \tag{20}$$

The characteristic matrix of the element is obtained by calculating the integrals of the shape function, and the mass matrix is as follows:

$$\begin{aligned} [M] &= \rho A\int_0^{\Delta x} N^T N dx \\ &= \rho A\begin{bmatrix} \frac{13\Delta x}{35} & \frac{11\Delta x^2}{210} & \frac{9\Delta x}{70} & \frac{-13\Delta x^2}{420} \\ \frac{11\Delta x^2}{210} & \frac{\Delta x^3}{105} & \frac{13\Delta x^2}{420} & \frac{-\Delta x^3}{140} \\ \frac{9\Delta x}{70} & \frac{13\Delta x^2}{420} & \frac{13\Delta x}{35} & \frac{-11\Delta x^2}{210} \\ \frac{-13\Delta x^2}{420} & \frac{-\Delta x^3}{140} & \frac{-11\Delta x^2}{210} & \frac{\Delta x^3}{105} \end{bmatrix}. \end{aligned} \tag{21}$$

Thus, the stiffness matrix of the unit can be obtained according to the above calculation. For the case of additional elastic elements in the unit (such as springs), this method is also applicable by simply adding the required stiffness factor to the corresponding position in the stiffness matrix.

$$\begin{aligned} [K] = EI&\begin{bmatrix} \frac{12}{\Delta x^3} & \frac{6}{\Delta x^2} & \frac{-12}{\Delta x^3} & \frac{6}{\Delta x^2} \\ \frac{6}{\Delta x^2} & \frac{4}{\Delta x} & \frac{-6}{\Delta x^2} & \frac{2}{\Delta x} \\ \frac{-12}{\Delta x^3} & \frac{-6}{\Delta x^2} & \frac{12}{\Delta x^3} & \frac{-6}{\Delta x^2} \\ \frac{6}{\Delta x^2} & \frac{2}{\Delta x} & \frac{-6}{\Delta x^2} & \frac{4}{\Delta x} \end{bmatrix} \\ - F&\begin{bmatrix} \frac{6}{5\Delta x} & \frac{1}{10} & \frac{-6}{5\Delta x} & \frac{1}{10} \\ \frac{1}{10} & \frac{2\Delta x}{15} & \frac{-1}{10} & \frac{-\Delta x}{30} \\ \frac{-6}{5\Delta x} & \frac{-1}{10} & \frac{6}{5\Delta x} & \frac{-1}{10} \\ \frac{1}{10} & \frac{-\Delta x}{30} & \frac{-1}{10} & \frac{2\Delta x}{15} \end{bmatrix}. \end{aligned} \tag{22}$$

The characteristic matrix of the bimorph can be described using an iterative method. When n=i+1, the mass matrix of the bimorph is

$$\begin{aligned} [M]_{bi} = &\begin{bmatrix} [M_i]_{2(i+1)\times 2(i+1)} & 0_{2(i+1)\times 2} \\ 0_{2\times 2(i+1)} & 0_{2\times 2} \end{bmatrix} \\ &+ \begin{bmatrix} 0_{2i\times 2i} & 0_{2i\times 4} \\ 0_{4\times 2i} & [M]_{4\times 4} \end{bmatrix}. \end{aligned} \tag{23}$$

For the cantilever boundary conditions, the first two rows and the first two columns in the above matrix are removed and the final mass matrix is obtained. The stiffness matrix is homogeneous. Moreover, the external excitation vector induced by the voltage is in the following form:

$$bE_3 d_{31} E_p h_p\left(h_s + h_p\right)\begin{bmatrix}0 & 1 & 0 & \cdots & 0 & -1\end{bmatrix}_{1\times 2(n+1)}^T. \tag{24}$$

3. Establishment of Finite Element Simulation

Combining the dynamics equation of the bimorph given by the finite element method, the characteristic matrix of the unit is assembled into the total matrix. Then the first two rows and the first two columns are removed from the total matrix. Therefore, the first-order natural frequency of the bimorph can be achieved, which is shown in Figure 2. The parameters of the bimorph can be obtained from [25].

Figure 3 shows the first-order natural frequency of the cantilever bimorph under different axial forces. In the numerical method, the bimorph is equally divided into 5 elements. The ANSYS simulation results are consistent with the numerical results.

In order to get the amplitude-frequency characteristics of the cantilever bimorph, the total characteristic matrix is constructed. For the cantilever condition, the final stiffness matrix $[K]_{bi}$ and the mass matrix $[M]_{bi}$ are obtained when the

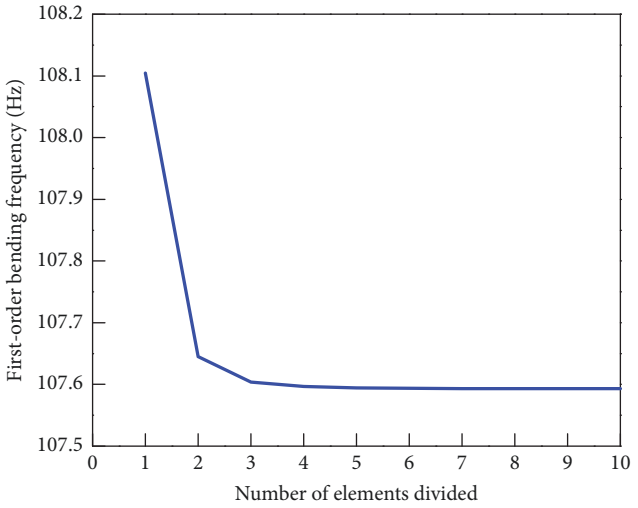

Figure 2: Convergence of first-order natural frequency.

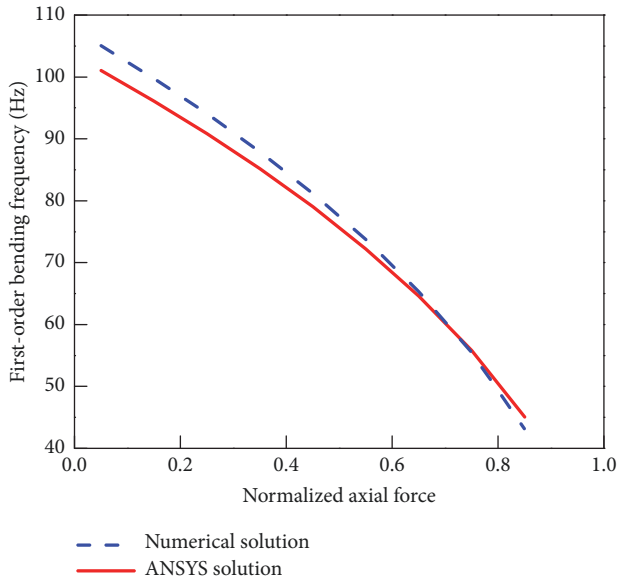

Figure 3: First-order natural frequency under different axial forces.

first two rows and the first two columns of the characteristic matrix are removed. Similarly, the first two rows in the excitation vector are removed. Thus, the following expression is achieved.

$$\{M_e\}_{bi} = bE_3 d_{31} E_p h_p \left(h_s + h_p\right) \left[0 \ \cdots \ 0 \ -1\right]^T. \quad (25)$$

The vibration equation of the cantilever bimorph is as follows:

$$[M]_{bi} \left\{\ddot{\delta}\right\} + [K]_{bi} \{\delta\} = bd_{31} E_p V \left(h_s + h_p\right) \left[0 \ \cdots \ 0 \ -1\right]^T. \quad (26)$$

Suppose the voltage is $V = v\sin(\omega t)$, the steady-state response can be obtained by solving (26).

$$\{\delta\} = bd_{31} E_p V \left(h_s + h_p\right) [H] \left[0 \ \cdots \ 0 \ -1\right]^T. \quad (27)$$

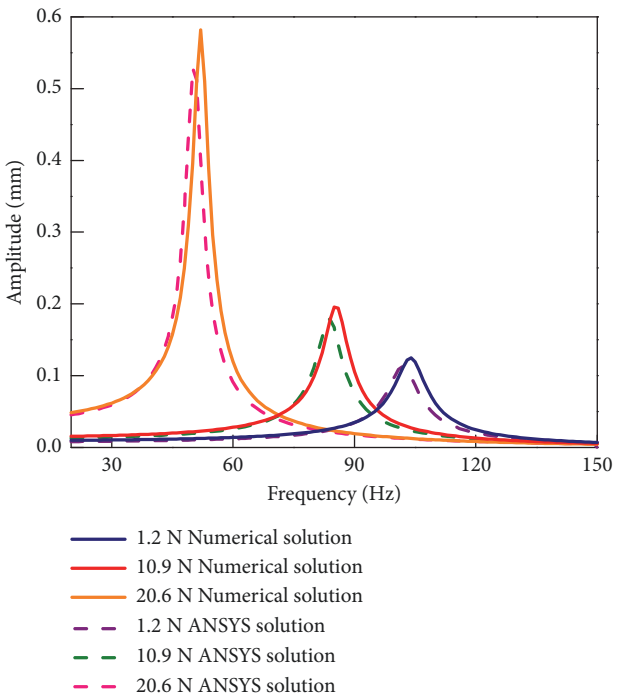

Figure 4: Amplitude-frequency characteristics under different axial forces.

The frequency response function is as follows:

$$[H] = \left(-\omega^2 [M]_{bi} + [K]_{bi}\right)^{-1}. \quad (28)$$

Finally, the amplitude of the cantilever bimorph is achieved.

$$A = \left[0 \ \cdots \ 0 \ \ 1 \ \ 0\right] bd_{31} E_p v \left(h_s + h_p\right) \cdot [H] \left[0 \ \cdots \ 0 \ -1\right]^T. \quad (29)$$

From formulae (27), (28), and (29), the amplitude of the free end at the voltage of 1 V is calculated. The results are compared with the ANSYS simulation results, as shown in Figure 4. It can be observed from the diagram that the first natural frequency of the bimorph decreases with the increase of axial force, whereas the amplitude gradually increases.

In order to analyze the transient characteristics of the bimorph, it is assumed that the voltage is a step signal.

$$V = \begin{cases} 0, & t < 0 \\ v, & t > 0. \end{cases} \quad (30)$$

The bimorph starts moving from the static state, and the unit impulse response of (26) can be obtained from the vibration theory as follows:

$$[h(t)] = [\Phi] \operatorname{diag}\left(\frac{\sin \omega_r t}{\omega_r}\right) [\Phi]^T \dot{\delta}_0. \quad (31)$$

where $[\Phi]$ is the mode matrix normalized by the main mass and ω_r is the r^{th} natural frequency of the bimorph. If damping is added, the unit impulse response can be expressed as

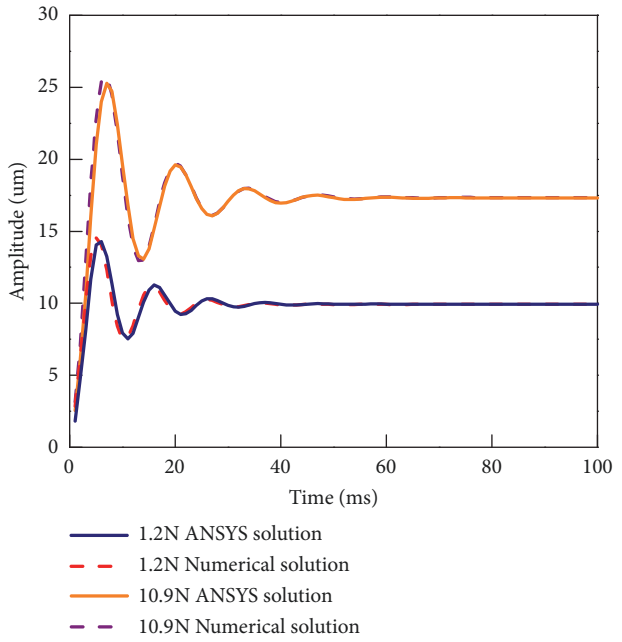

Figure 5: Step response of the bimorph under different axial forces.

$$[h(t)] = [\Phi]\,\mathrm{diag}\left(\frac{e^{-\zeta\omega_r t}\sin\sqrt{1-\zeta^2}\omega_r t}{\omega_r\sqrt{1-\zeta^2}}\right)[\Phi]^T\dot{\delta}_0, \quad (32)$$

where ζ is the damping ratio. The zero-initial state step response of the undamped bimorph can be obtained using Duhamel's integral.

$$\begin{aligned}\{\delta(t)\} &= \int_0^t [h(t)]\{M_e\}_{bi}\,dt \\ &= bd_{31}E_p v\left(h_s+h_p\right)[\Phi]\,\mathrm{diag}\left(\frac{1-\cos\omega_r t}{\omega_r^2}\right) \\ &\quad\cdot[\Phi]^T\begin{bmatrix}0 & \cdots & 0 & -1\end{bmatrix}^T.\end{aligned} \quad (33)$$

Further, the step response of a damped zero-initial state is

$$\begin{aligned}\{\delta(t)\} &= bd_{31}E_p v\left(h_s+h_p\right)[\Phi]\,\mathrm{diag}\left(V_r\right) \\ &\quad\cdot[\Phi]^T\begin{bmatrix}0 & \cdots & 0 & -1\end{bmatrix}^T,\end{aligned} \quad (34)$$

where

$$V_r(t) = \frac{\sqrt{1-\zeta^2}-e^{-\zeta\omega_r t}\left(\zeta\sin\left(\sqrt{1-\zeta^2}\omega_r t\right)+\sqrt{1-\zeta^2}\cos\left(\sqrt{1-\zeta^2}\omega_r t\right)\right)}{\omega_r^2\sqrt{1-\zeta^2}}. \quad (35)$$

By solving the diagonal matrix $\mathrm{diag}(\omega_r)$ constructed using generalized eigenvalues and the characteristic matrix $[\Phi]$, the following equations are established. Subsequently, $[\Phi]$ is normalized by the main mass, and the unit matrix $[\Phi]^T[M]_{bi}[\Phi]$ is obtained.

$$[K]_{bi}[\Phi] = [M]_{bi}[\Phi]\,\mathrm{diag}\left(\omega_r\right). \quad (36)$$

The step response of the bimorph at different axial forces is calculated from (34). The transient dynamic analysis with precompression is performed using ANSYS software, and the equivalent torque is added in the simulation.

$$M_e = bd_{31}E_p v\left(h_s+h_p\right). \quad (37)$$

The voltage is set to 1 V and the amplitude of the free end can be obtained under different axial forces, as shown in Figure 5. It can be seen that the ANSYS simulation results are consistent with the numerical calculation results, and the response time in the no-load state is of the order of milliseconds. The axial force can apparently enlarge the displacement output but has little effect on the response time of the bimorph.

4. Experiments of Piezoelectric Bimorph

4.1. Static Experiment of Piezoelectric Bimorph. As shown in Figure 6, a clamping device is designed for the installation of the piezoelectric bimorph. The axial force was changed by increasing or decreasing the weights in the experiment. The deflection of the bimorph was tested using the laser displacement sensor.

In the experiment, the voltage of the upper and lower surfaces was supplied by the DC power, and the substrate layer was grounded. The buckling critical load of the cantilever bimorph was calculated to be 36 N by using formula (9). The maximum static deflection under the axial forces of 0 N and 16 N are shown in Figure 7.

The analytical solution in Figure 7 is obtained from (8). It can be seen that when the axial force is constant, the deformation is linear with the voltage. The axial force can evidently amplify the displacement output, and the maximum deflection of the bimorph under an axial force of 16 N has increased by approximately 30%. The experimental results and the numerical results obtained using formula (8) are very close when no axial force is applied. Even under large axial force, the theoretical and experimental results are basically the same.

4.2. Modal Experiment of Piezoelectric Bimorph. The modal experiment of the piezoelectric bimorph mainly tests its amplitude-frequency characteristics, natural frequencies, and natural modes under different axial forces. The amplitude of the piezoelectric material is in the micron range, and the one-dimensional out-of-plane vibration is often measured using a laser Doppler vibrometer. Therefore, the PSV-300F-B

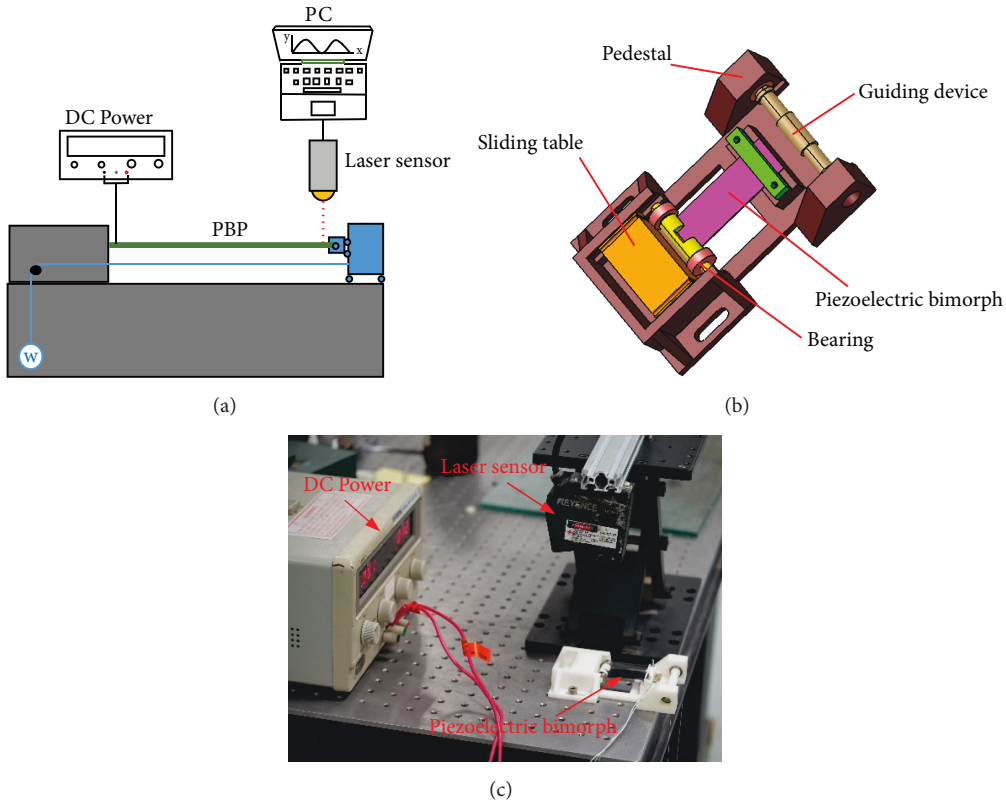

Figure 6: Static experiment of precompressed cantilever piezoelectric bimorph: (a) experiment system; (b) clamping device; (c) experimental devices.

Table 1: First-order natural frequency of the cantilever bimorphs with different axial forces.

Axial force (N)	0	2	10
Numerical results (Hz)	144	138	125
Experimental results (Hz)	150	129	96

laser scanning Doppler vibration measurement was used to conduct the modal experiments on the bimorph.

In the experiment, the excitation voltage amplitude was 30 V and the axial forces were 0 N, 2 N, and 10 N. The experimental and numerical results are shown in Table 1. As the damping of the bimorph cannot be ignored, the proportional damping matrix (calculated using (38)) is added to the numerical calculation, and the damping ratio is set to ζ=0.02.

$$[C]_{bi} = \left([\Phi]_{bi}^{T}\right)^{-1} \operatorname{diag}\left(2M_r\omega_r\zeta\right)[\Phi]_{bi}^{-1}. \tag{38}$$

From the experimental results, it can be observed that the natural frequency of the bimorph gradually decreases with the increase in the axial force, but its bandwidth can still reach 96 Hz with an axial prepressure of 10 N, which has a significant advantage over the traditional electromagnetic actuator.

The resonant frequency of the bimorph calculated using the numerical method is very similar to the experimental result when the axial force is not applied. With the increase of the axial force, the experimental results of the first-order natural frequency are relatively smaller than the numerical calculation results, which may be related to additional factors generated by the instruments in the experiment. However, the trends in the results are the same.

5. Conclusion

In this study, the rigid-flexible coupling dynamic model of the piezoelectric bimorph is established by using the theoretical tools of analytical mechanics, structural dynamics, and finite element method. The force-displacement characteristics under different axial forces are analyzed, and the frequency response function is given. The steady-state and transient responses of the bimorph are analyzed. Simultaneously, according to the theoretical analysis above, the corresponding code is written using MATLAB software. Finally, the experimental platform is set up to study the static and dynamic characteristics of the axially precompressed bimorph. The results show that increase of axial force has a significant amplification effect on the steady-state response amplitude of the displacement, and it reduces the resonance frequency. However, the resonance frequency can still reach 60 Hz and the displacement output is amplified by nearly 30% while 0.6 times the buckling critical load is applied. The response time is still in the millisecond range under a large

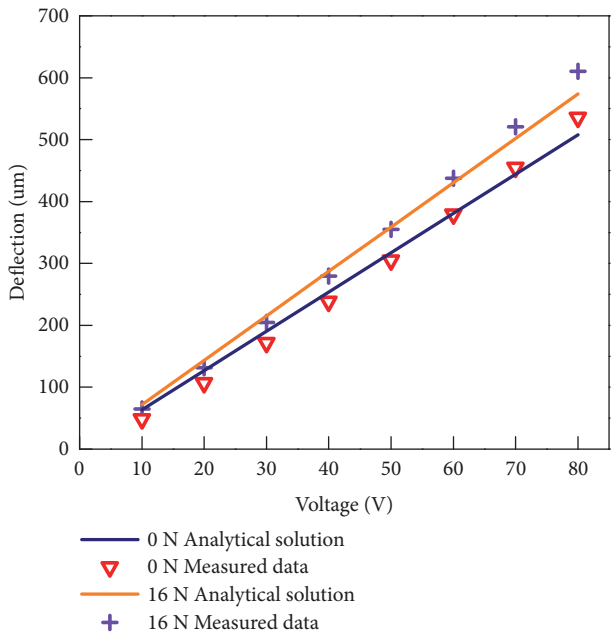

FIGURE 7: Deflection of bimorph under different voltages and axial forces.

axial force, which indicates that the bimorph has excellent dynamic characteristics as an actuator. This article provides a solid theoretical basis for the design of the PBP servo system.

Data Availability

All the data used to support the findings of this study are included within the article and are reflected in the form of figures or tables.

Conflicts of Interest

The authors declare that they have no conflicts of interest.

Acknowledgments

This research is supported by National Natural Science Foundation of China (Grant no. 51575259), National Basic Research Program (973 Program) (2015CB057500), the Funding of Jiangsu Innovation Program for Graduate Education (nos. KYLX_0236 and KYLX15_0226), and the Fundamental Research Funds for the Central Universities (no. NS2015004).

References

[1] M. Rushdi, T. Tennakoon, K. Perera, A. Wathsalya, and S. R. Munasinghe, "Development of a small-scale autonomous UAV for research and development," in *Proceedings of the 2016 IEEE International Conference on Information and Automation for Sustainability (ICIAfS)*, pp. 1–6, Galle, Sri Lanka, December 2016.

[2] O. Bilgen and M. I. Friswell, "Piezoceramic composite actuators for a solid-state variable-camber wing," *Journal of Intelligent Material Systems and Structures*, vol. 25, no. 7, pp. 806–817, 2014.

[3] C. Zhao, *Ultrasonic Motors*, Science Press, 2010.

[4] A. Henke, M. A. Kümmel, and J. Wallaschek, "A piezoelectrically driven wire feeding system for high performance wedge-wedge-bonding machines," *Mechatronics*, vol. 9, no. 7, pp. 757–767, 1999.

[5] J. C. Gomez and E. Garcia, "Morphing unmanned aerial vehicles," *Smart Materials and Structures*, vol. 20, no. 10, Article ID 103001, 2011.

[6] D. Karagiannis, D. Stamatelos, V. Kappatos, and T. Spathopoulos, "An investigation of shape memory alloys as actuating elements in aerospace morphing applications," *Mechanics of Advanced Materials and Structures*, vol. 24, no. 8, pp. 647–657, 2017.

[7] R. Barrett, "Adaptive fight control actuators and mechanisms for missiles, munitions and uninhabited aerial vehicles (UAVs)," in *Advances in Flight Control Systems*, InTech, 2011.

[8] R. Wlezien, G. Horner, A. McGowan et al., The Aircraft Morphing Program. 98-1927. 1998.

[9] P. C. Chen, E. Sulaeman, D. D. Liu, and L. M. Auman, "Body-flexure control with smart actuation for hypervelocity missiles," in *Proceedings of the 44th AIAA/ASME/ASCE/AHS/ASC Structures, Structural Dynamics, and Materials Conference*, pp. 5157–5167, USA, April 2003.

[10] X. Zhang, W. Wang, and G. H. Zong, "The application of piezoelectric actuator for small aircraft," *Advanced Materials Research*, vol. 998-999, pp. 674–677, 2014.

[11] R. M. Barrett and P. Tiso, "Actuator," 1 Mar 2011, US Pat 7,898,153.

[12] E. F. Crawley, "Intelligent structures for aerospace: a technology overview and assessment," *AIAA Journal*, vol. 32, no. 8, pp. 1689–1699, 1994.

[13] F. S. Huang, Z. H. Feng, Y. T. Ma et al., "High-frequency performance for a spiral-shaped piezoelectric bimorph," *Modern Physics Letters B. Condensed Matter Physics, Statistical Physics, Atomic, Molecular and Optical Physics*, vol. 32, no. 10, Article ID 1850111, 2018.

[14] A. Erturk and D. J. Inman, "An experimentally validated bimorph cantilever model for piezoelectric energy harvesting from base excitations," *Smart Materials and Structures*, vol. 18, no. 2, Article ID 025009, 2009.

[15] S. R. Hall and E. F. Prechtl, "Development of a piezoelectric servoflap for helicopter rotor control," *Smart Materials and Structures*, vol. 5, no. 1, pp. 26–34, 1996.

[16] R. J. Wood, S. Avadhanula, E. Steltz et al., "Design, fabrication and initial results of a 2g autonomous glider," in *Proceedings of the IECON 2005: 31st Annual Conference of IEEE Industrial Electronics Society*, pp. 1870–1877, November 2005.

[17] G. A. Lesieutre and C. L. Davis, "Can a coupling coefficient of a piezoelectric device be higher than those of its active material?" *Journal of Intelligent Materials Systems and Structures*, vol. 8, pp. 859–867, 1997.

[18] G. A. Lesieutre and C. L. Davis, "Transfer having a coupling coefficient higher than its active material," 22 May 2011, US Pat 6,236,143.

[19] R. Vos and R. Barrett, "Post-buckled precompressed (PBP) piezoelectric actuators for UAV flight control," in *Proceedings of SPIE - The International Society for Optical Engineering*, vol. 6173, pp. 1–12, 2006.

[20] R. Barrett, R. McMurtry, R. Vos, P. Tiso, and R. De Breuker, "Post-buckled precompressed piezoelectric flight control actuator design, development and demonstration," *Smart Materials and Structures*, vol. 15, no. 5, pp. 1323–1331, 2006.

[21] R. De Breuker, P. Tisot, R. Vos, and R. Barrett, "Nonlinear semi-analytical modeling of Post-Buckled Precompressed (PBP) piezoelectric actuators for UAV flight control," in *Proceedings of the 47th AIAA/ASME/ASCE/AHS/ASC Structures, Structural Dynamics and Materials Conference*, vol. 1795, pp. 2461–2473, USA, May 2006.

[22] G. Giannopoulos, J. Monreal, and J. Vantomme, "Snap-through buckling behavior of piezoelectric bimorph beams: I. analytical and numerical modeling," *Smart Materials and Structures*, vol. 16, no. 4, pp. 1148–1157, 2007.

[23] G. Giannopoulos, J. Monreal, and J. Vantomme, "Snap-through buckling behavior of piezoelectric bimorph beams: II. experimental verification," *Smart Materials and Structures*, vol. 16, no. 4, pp. 1158–1163, 2007.

[24] D. V. Hutton, *Fundamentals of Finite Element Analysis*, New York, NY, USA, 2004.

[25] H. Chen, J. Wang, C. Chen, S. Liu, and H. Chen, "Dynamic modeling and characteristic analysis of piezoelectric rudder actuator," *Review of Scientific Instruments*, vol. 90, no. 1, Article ID 016102, 2019.